



## Digital Logic Gate Using Quantum-Dot Cellular Automata

Islamshah Amlani, *et al.*

*Science* **284**, 289 (1999);

DOI: 10.1126/science.284.5412.289

**The following resources related to this article are available online at [www.sciencemag.org](http://www.sciencemag.org) (this information is current as of March 31, 2007):**

**Updated information and services**, including high-resolution figures, can be found in the online version of this article at:

<http://www.sciencemag.org/cgi/content/full/284/5412/289>

This article has been **cited by** 107 article(s) on the ISI Web of Science.

This article has been **cited by** 5 articles hosted by HighWire Press; see:

<http://www.sciencemag.org/cgi/content/full/284/5412/289#otherarticles>

This article appears in the following **subject collections**:

Physics, Applied

[http://www.sciencemag.org/cgi/collection/app\\_physics](http://www.sciencemag.org/cgi/collection/app_physics)

Information about obtaining **reprints** of this article or about obtaining **permission to reproduce this article** in whole or in part can be found at:

<http://www.sciencemag.org/about/permissions.dtl>

# Digital Logic Gate Using Quantum-Dot Cellular Automata

Islamshah Amlani,<sup>1\*</sup> Alexei O. Orlov,<sup>1</sup>  
Geza Toth,<sup>1,2</sup> Gary H. Bernstein,<sup>1</sup> Craig S. Lent,<sup>1</sup>  
Gregory L. Snider<sup>1</sup>

A functioning logic gate based on quantum-dot cellular automata is presented, where digital data are encoded in the positions of only two electrons. The logic gate consists of a cell, composed of four dots connected in a ring by tunnel junctions, and two single-dot electrometers. The device is operated by applying inputs to the gates of the cell. The logic AND and OR operations are verified using the electrometer outputs. Theoretical simulations of the logic gate output characteristics are in excellent agreement with experiment.

Field-effect transistors (FETs) are the foundation of present digital logic technologies such as complementary metal oxide semiconductors. Despite vast improvements in integrated circuit fabrication technology over the past three decades, the role played by the FET has remained that of a current switch, much like the mechanical relays used by Konrad Zuse in the 1930s. By adhering to strict scaling rules, FETs have maintained acceptable performance despite tremendous reductions in size, permitting the microelectronics industries to make phenomenal increases in device density and computational power. As device feature sizes approach quantum limits, fundamental effects will make further scaling difficult, requiring a departure from the FET-based paradigm and necessitating revolutionary approaches to computing. The approach must be compatible with the inherent properties of nanostructures, as it should exploit the effects that accompany small sizes. An alternate paradigm is that of quantum-dot cellular automata (QCA) (1–3), which uses the arrangements of individual electrons, instead of currents and voltages, to encode binary information.

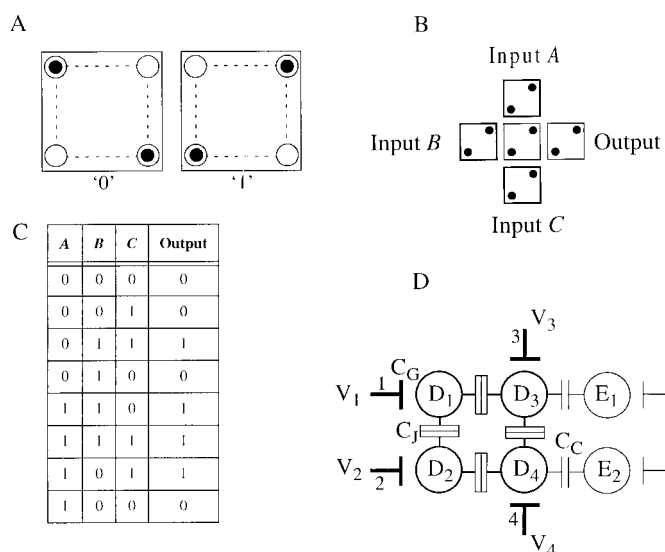
QCA is a nanostructure-compatible computation paradigm that uses arrays of quantum-dot cells to implement digital logic functions. A key element of this paradigm is a QCA cell, which consists of four dots located at the vertices of a square (Fig. 1A); such a cell was experimentally demonstrated (4). When the cell is charged with two excess electrons, they occupy diagonal sites as a result of mutual electrostatic repulsion. The two diagonal polarizations are energetically equivalent ground states of the cell, and are used to represent logic 0 and logic 1. A

polarization change in a QCA cell is induced by causing an electron to switch positions in one set of dots, thus inducing an opposite electron switch in an adjacent set of dots, resulting in a change of the electron arrangement from one diagonal to the other.

The fundamental QCA logic device is a three-input majority logic gate (Fig. 1B) consisting of an arrangement of five standard cells: a central logic cell, three inputs labeled *A*, *B*, and *C*, and an output cell. The polarization states of inputs *A*, *B*, and *C* determine that of the logic cell, which can assume either polarization, while the output polarization follows that of the logic cell. In operation, the polarization of the logic cell becomes that of the majority of the three input cells. QCA logic gates can be cascaded, so that in a more complex QCA circuit, the three inputs would be driven by the outputs of previous gates. Similarly, the output of the majority gate can be connected to drive a subsequent stage of logic gates (5).

A majority gate can be programmed to act

**Fig. 1.** (A) QCA cell showing two possible polarizations. (B) QCA majority gate, the fundamental logic element of the QCA paradigm. (C) Truth table containing all possible input combinations in Gray code, and majority gate outputs. (D) Schematic of our QCA system. The cell is defined by dots  $D_1$  to  $D_4$  connected in a ring by tunnel junctions. Dots  $D_3$  and  $D_4$  are capacitively coupled to electrometer dots  $E_1$  and  $E_2$ , respectively. External leads and tunnel junctions for the cell and the electrometers are not shown.



<sup>1</sup>Department of Electrical Engineering, University of Notre Dame, Notre Dame, IN 46556, USA. <sup>2</sup>Neuromorphic Information Technology Graduate Center, Budapest, Kende-u.13, H-1111, Hungary.

\*To whom correspondence should be addressed. E-mail: islamshah.amlani.1@nd.edu

as an OR gate or an AND gate by fixing any one of the three inputs as a program line. If the programming input is a 0, the AND operation is performed on the remaining two inputs. If the programming input is a 1, the OR operation is performed on the other two inputs (Fig. 1C).

Although QCA architecture can be implemented in many systems, we choose the metal tunnel junction implementation described by Lent and Tougaw (3). In our QCA system (Fig. 1D), the cell consists of four small Al islands (“dots”),  $D_1$  to  $D_4$ , connected in a ring by  $\text{AlO}_x$  tunnel junctions. In initial biasing of the cell, two excess electrons enter the cell through tunnel junctions, which for simplicity are not shown. A complete schematic for a related experiment has been published (4). Junction capacitances  $C_j$  are sufficiently small to ensure charge quantization on each dot at cryogenic temperatures (6). Each dot is also capacitively coupled to a gate, via capacitance  $C_G$ , that influences the charge state of its respective dot. To determine the cell polarization, we measure electrostatic potentials on islands  $D_3$  and  $D_4$  using capacitively coupled single dots,  $E_1$  and  $E_2$ , as noninvasive electrometers (7, 8).

Nanometer-scale  $\text{Al}/\text{AlO}_x/\text{Al}$  tunnel junctions are fabricated using the standard Dolan-bridge technique (9). Aluminum islands and leads are defined by electron beam lithography and subsequent shadow evaporation processes with an intermediate in situ oxidation step. The experiment is performed in a dilution refrigerator with an ambient magnetic field of 1 T to suppress the superconductivity of Al metal. All relevant capacitances are extracted from measurements of Coulomb blockade oscillations (4), and are used in theoretical simulations of the device characteristics using classical Coulomb blockade theory. The effects of unintentional cross-talk capacitances between each gate and all nonadjacent dots are compensated using feedback circuitry (10).

**Fig. 2.** Experimental setup for majority gate demonstration. Inputs *A*, *B*, and *C* (shaded at left) are replaced by potential shifts on the gates (shaded at right) that are equivalent to polarization states of the input cells.

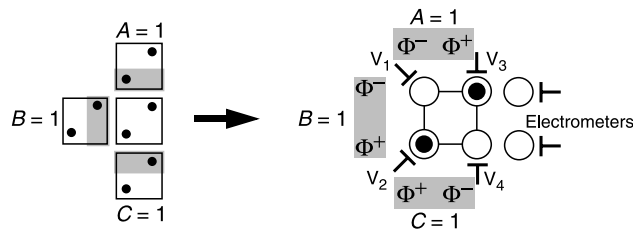
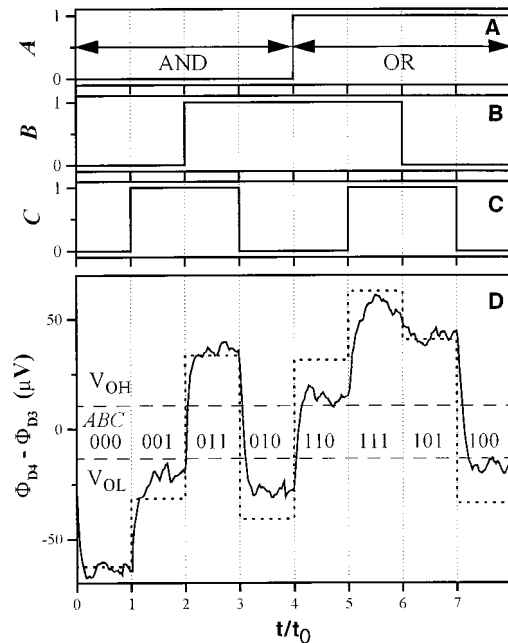


**Fig. 3.** Demonstration of majority gate operation. (A to C) Inputs in Gray code. The first four and last four inputs illustrate AND and OR operations, respectively. (D) Output characteristic of majority gate where  $t_0 = 20$  s is the input switching period. The dashed line shows the theory for 70 mK; the solid line represents the measured data. Output high ( $V_{OH}$ ) and output low ( $V_{OL}$ ) levels are marked by dashed lines.



First, the logic cell is biased using gates 1 to 4 in an unpolarized state where logic 1 and 0 are equally probable (4), and the electrometer outputs are set to 0 V for this condition. This procedure also cancels the effect of the substrate background charge. Figure 2 shows the correspondence between the representation on the left and the configuration of our majority gate experiment on the right. Differential signals *A* (between gates 1 and 3), *B* (between gates 1 and 2), and *C* (between gates 2 and 4) constitute the inputs to the central cell. The negative (positive) bias on a gate,  $\Phi^-$  ( $\Phi^+$ ), mimics the presence (absence) of an electron in the input dots, as shown by the shaded regions in Fig. 2. The amplitudes of  $\Phi^-$  and  $\Phi^+$  are carefully chosen to mimic the potentials due to the polarization of an input cell while they remain small enough not to change the number of excess electrons in the cell.

Differential signals *A*, *B*, and *C* are converted into logic levels 1 and 0 on the basis of the convention used in Fig. 1A. As dots  $D_1$  and  $D_2$  are coupled to only one gate electrode each, voltages corresponding to inputs *A* and *B* on gate 1, and inputs *B* and *C* on gate 2, are added in order to mimic the effect of two input dots. For instance, the input configuration shown in Fig. 2 ( $ABC = 111$ ) is achieved by setting  $V_1 = 2\Phi^-$ ,  $V_2 = 2\Phi^+$ ,  $V_3 = \Phi^+$ , and  $V_4 = \Phi^-$ .

With inputs *A*, *B*, and *C* traced as a function of time (Fig. 3, A to C) according to the truth table in Fig. 1C, the differential potential between dots  $D_4$  and  $D_3$ ,  $\Phi_{D4} - \Phi_{D3}$ , is measured using the electrometers  $E_2$  and  $E_1$  (Fig. 3D). (The transient characteristics are determined by the time constant of our electrometer circuitry.)

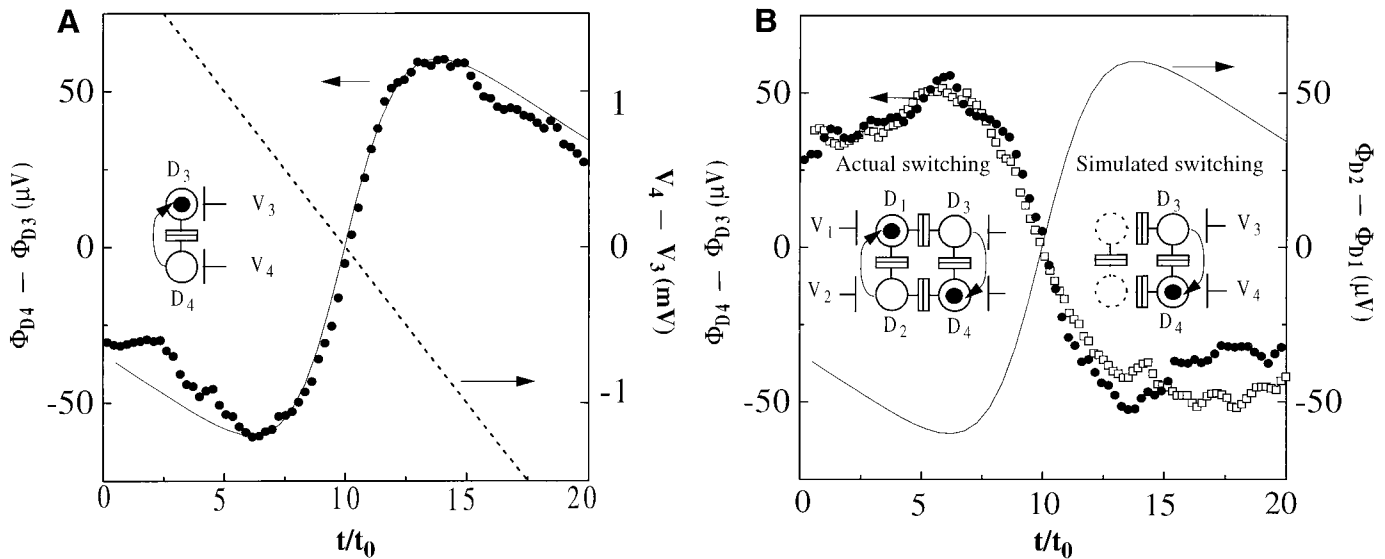


**Fig. 4.** (A) Differential potential change on the dots as an electron switches from  $D_4$  to  $D_3$ . The dashed line represents the differential input voltage applied to gates 3 and 4 as a function of time. Solid circles show the measured data and the solid line represents the theoretical prediction for 70 mK;  $t_0 = 15$  s. (B) Switching induced in  $D_3D_4$  by two mechanisms. Solid circles show the measured differential

potential change of  $D_3D_4$  caused by the simulated dot potential, as depicted by inset at right. The solid line shows the differential potential applied between gates 4 and 3 (scaled by  $C_1/C_3$ ). Open squares show the measured differential potential change of  $D_3D_4$  caused by an electron switching in  $D_1D_2$ , as depicted by inset at left;  $t_0 = 15$  s.

The theoretical results (dashed line in Fig. 3D) are calculated for the electron temperature in the experiment (70 mK), as determined from the temperature dependence of Coulomb blockade oscillations ( $I$ ). Although no adjustable parameters are used in the theory, the agreement between the experimental and theoretical results is excellent. The output high ( $V_{OH}$ ) and output low ( $V_{OL}$ ) show a clear separation, as required for digital logic. The first and last four input steps are grouped separately, with  $A$  as the programming input, to illustrate AND and OR operations. The AND operation is carried out for  $A = 0$ , for which we see that the output is high only when the remaining two inputs are also high. The OR operation is performed when  $A = 1$ , for which the output is high when either of the other two inputs is high. These data confirm majority gate operation and thus demonstrate a logic gate that requires only two electrons to function.

The gap between  $V_{OH}$  and  $V_{OL}$  would be larger for either lower temperatures or smaller capacitances. Thermal smearing of the charge states of the dots results in a less than complete polarization of the cell. Therefore, the performance of the gate could be improved by lowering the temperature. However, a better way is to reduce the dot capacitance (by reducing the size of the dots), which will raise the energy of the excited states. When all capacitances are reduced by a factor of 10, the calculated output characteristic shows increased separation between  $V_{OH}$  and  $V_{OL}$  and negligible output deviations for all input combinations. QCA logic gates using a molecular implementation will not only yield greater performance, but will also operate at room temperature (12).

Some key issues must be addressed to determine the response of the majority gate when it is integrated in a real QCA circuit. In QCA arrays, each cell responds to the polarizations of neighboring cells. Therefore, we must justify that the voltages applied to the central cell gates in our majority gate experiment produce the same effects as electrons switching in neighboring cells.

We performed two experiments to demonstrate that our input voltages have the same effect as that of actual electron switching in input cells  $A$ ,  $B$ , and  $C$ . First, we found the potential swing due to an electron switching from one dot to another. We applied a differential voltage between gates 3 and 4 ( $V_3 = -V_4$ ) to induce electron switching in  $D_3D_4$  (inset, Fig. 4A). As an electron moves from  $D_4$  to  $D_3$ , the potential of the bottom dot undergoes a positive shift due to removal of an electron, while the potential of the top dot undergoes a negative shift due to addition of an electron. The differential potential swing ( $\Phi_{D_4} - \Phi_{D_3}$ ) for this switching is positive (Fig. 4A), with theory closely matching the measured data [the calculated differential potential swing ( $\Phi_{D_2} - \Phi_{D_1}$ ) is the same when the bias is applied

between gates 1 and 2]. The input signals applied to the gates in the majority gate demonstration (Fig. 3) have the same amplitudes as that shown in Fig. 4A, scaled by  $C_j/C_G$  to compensate for differences in capacitance.

Next, to demonstrate that the application of "simulated" dot potentials to the gates of the cell mimics an electron switching in a neighboring cell, we applied the differential potential extracted in the previous experiment directly to gates 3 and 4 (with the weighting factor  $C_j/C_G$ ) and measured the differential potentials between  $D_3$  and  $D_4$ . This result is compared to that due to an actual electron switching in nearby dots  $D_1D_2$ . Figure 4B shows the change in differential potential of  $D_3D_4$  caused by the two mechanisms as a function of time (insets, Fig. 4B), with the data confirming that the response of  $D_3D_4$  is similar when switched by either the simulated potential or a real electron. This is as expected because charge modulations induced on  $D_3D_4$  by the two mechanisms are the same; that is,  $V_3C_G = \Phi_{D_1}C_j$  and  $V_4C_G = \Phi_{D_2}C_j$ . These results confirm that using the simulated dot potentials for the inputs in our majority gate experiment is indeed a reliable indicator of how a majority gate would respond when integrated in a QCA circuit.

References and Notes

1. C. S. Lent and P. D. Tougaw, *Proc. IEEE* **85**, 541 (1997).
2. ———, W. Porod, *Appl. Phys. Lett.* **62**, 714 (1993).
3. C. S. Lent and P. D. Tougaw, *J. Appl. Phys.* **75**, 4077 (1994).
4. A. O. Orlov, I. Amlani, G. H. Bernstein, C. S. Lent, G. L. Snider, *Science* **277**, 928 (1997); I. Amlani, A. O. Orlov, G. L. Snider, C. S. Lent, G. H. Bernstein, *Appl. Phys. Lett.* **72**, 2179 (1998).
5. In an integrated QCA circuit, a clocking scheme is used to control the direction of information flow. See (7).
6. K. K. Likharev, *IBM J. Res. Dev.* **42**, 144 (1988).
7. P. Lafarge *et al.*, *Z. Phys. B* **85**, 327 (1991); I. Amlani, A. O. Orlov, C. S. Lent, G. L. Snider, G. H. Bernstein, *Appl. Phys. Lett.* **71**, 1730 (1997).
8. G. L. Snider *et al.*, unpublished data; G. H. Bernstein, I. Amlani, A. O. Orlov, C. S. Lent, G. L. Snider, unpublished data.
9. T. A. Fulton and G. H. Dolan, *Phys. Rev. Lett.* **58**, 109 (1987).
10. G. L. Snider *et al.*, *Solid State Electron.* **42**, 1355 (1998).
11. H. Grabert and M. H. Devoret, Eds., *Single Electron Tunneling* (Plenum, New York, 1992), p. 181.
12. C. S. Lent, P. D. Tougaw, W. Porod, *Proceedings of Workshop on Physics and Computation* (IEEE Computer Press, Los Alamitos, CA, 1994), vol. 5.
13. Supported in part by the Defense Advanced Research Projects Agency, the Office of Naval Research (grant N0014-95-1-1166), and NSF. We thank W. Porod and J. Merz for helpful discussions.

24 November 1998; accepted 19 February 1999

# Remote Triggering of Waves in an Electrochemical System

J. Christoph, P. Strasser,\* M. Eiswirth, G. Ertl

In the potentiostatic electrochemical oxidation of formic acid on a platinum ring electrode under bistable conditions, an appropriate perturbation at one location of the ring can cause the emergence of a wave on the opposite side (remote triggering). These findings can be rationalized in terms of the nonlocal coupling function of the system and are theoretically reproduced by solution of the corresponding reaction-migration equation.

Trigger waves are a widespread phenomenon, both in conservative systems (such as ripples on the surface of water) and in dissipative systems [such as active chemical media (1), nerve axons, or heart tissue (2, 3)]. They typically originate from the location where a perturbation (trigger) has been applied, be it a stone thrown into a pond or an electrical stimulus applied to an axon. If, however, coupling between different parts is nonlocal, that is, when any change of state affects instantaneously the whole system (4, 5), the necessity for local causality will no longer exist. We present here the results and theoretical interpretation of an electrochemical experiment in which a local perturbation causes the initiation of a trigger wave in a remote region.

Fritz-Haber-Institut der Max-Planck-Gesellschaft, Faradayweg 4-6, D-14195 Berlin, Germany.

\*To whom correspondence should be addressed. E-mail: strasser@fhi-berlin.mpg.de

The experiment was performed with the electrochemical oxidation of formic acid on platinum (6), which exhibits for a certain range of parameters bistability between a passive (OH-poisoned) and an active (high-current)

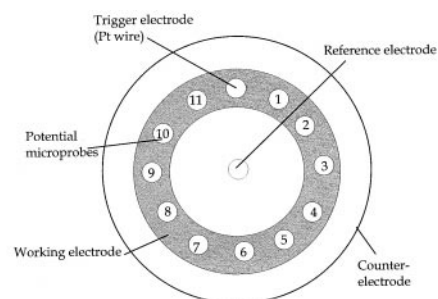


Fig. 1. Schematic view of the electrode setup. The potential microprobes (1 through 11) are separated by 30° angles, and the perturbations were applied with a Pt wire.